Atmospheric Research 181 (2016) 1–11

Contents lists available at ScienceDirect

Atmospheric Research

journal homepage: www.elsevier.com/locate/atmosres

A quantitative comparison of precipitation forecasts between the storm-scale numerical weather prediction model and auto-nowcast system in Jiangsu, China

Gaili Wang [a,b,*], Ji Yang [b], Dan Wang [c], Liping Liu [a]

[a] State Key Laboratory of Severe Weather, Chinese Academy of Meteorological Science, 46 Zhongguancun South Street, Haidian District, Beijing 100081, China
[b] Jiangsu Institute of Meteorological Science, 16 Kunlun Load, Nanjing, Jiangsu 210009, China
[c] National Meteorological Center, China Meteorological Administration, 46 Zhongguancun South Street, Haidian District, Beijing 100081, China

ARTICLE INFO

Article history:
Received 26 February 2016
Received in revised form 31 May 2016
Accepted 6 June 2016
Available online 7 June 2016

Keywords:
Beijing auto-nowcast system
ARPS forecasts
Forecast performances
Gridpoint-based measures
Object-based verification

ABSTRACT

Extrapolation techniques and storm-scale Numerical Weather Prediction (NWP) models are two primary approaches for short-term precipitation forecasts. The primary objective of this study is to verify precipitation forecasts and compare the performances of two nowcasting schemes: a Beijing Auto-Nowcast system (BJ-ANC) based on extrapolation techniques and a storm-scale NWP model called the Advanced Regional Prediction System (ARPS). The verification and comparison takes into account six heavy precipitation events that occurred in the summer of 2014 and 2015 in Jiangsu, China. The forecast performances of the two schemes were evaluated for the next 6 h at 1-h intervals using gridpoint-based measures of critical success index, bias, index of agreement, root mean square error, and using an object-based verification method called Structure-Amplitude-Location (SAL) score. Regarding gridpoint-based measures, BJ-ANC outperforms ARPS at first, but then the forecast accuracy decreases rapidly with lead time and performs worse than ARPS after 4–5 h of the initial forecast. Regarding the object-based verification method, most forecasts produced by BJ-ANC focus on the center of the diagram at the 1-h lead time and indicate high-quality forecasts. As the lead time increases, BJ-ANC overestimates precipitation amount and produces widespread precipitation, especially at a 6-h lead time. The ARPS model overestimates precipitation at all lead times, particularly at first.

1. Introduction

Heavy rain is one of the most severe weather systems in China, and causes severe flooding and other disaster events such as landslides. High-resolution quantitative precipitation forecasts (QPFs) with a lead time of a few hours, referred to as "nowcasting," plays an important role in flash flood warning and emergency response.

Heavy rain is one of the most severe weather systems in China causing flood and other hydrological disaster events. Currently, nowcasting of precipitation relies on extrapolation techniques for their quick computational skills. A common technique considers radar echo movements between two consecutive radar patterns and extrapolates the radar patterns. Examples include the method of tracking radar echoes by correlation (TREC) and McGill algorithm for precipitation nowcasting by Lagrangian extrapolation (Rinehart and Garvey, 1978; Germann and Zawadzki, 2004). The second technique identifies storms as 3D objects and tracks and forecasts storm-related characteristics including storm area, mass centroids, and maximum reflectivity (Dixon and Wiener, 1993; Johnson et al., 1998; Vila et al., 2008). As the forecast performances of these extrapolation methods decrease rapidly with increasing lead time, more comprehensive nowcasting systems that use prediction factors from various sources and that predict the future evolution of precipitation have been run operationally; these systems include the Auto-Nowcast (ANC, Mueller et al., 2003), Generating Advanced Nowcasts for Development in Operational Land-surface Flood forecasts (GANDOLF, Pierce et al., 2000), and Short-range Warning of Intense Rainstorms in Localized System (SWIRLS, Li and Lai, 2004). ANC identifies boundary layer convergence lines to predict storm initiation, growth, and dissipation and combines predictor fields from various observations (radar, satellite, sounding, mesonet, and profiler), forecaster input, and feature detection algorithms to produce short-term (0 − 1 h) nowcasts of the storm. GANDOLF distinguishes stratiform and convective precipitations. Extrapolation of radar echoes are merged with the NWP model for stratiform precipitation, and an object-oriented conceptual model is explored to model storm development for convective precipitation. SWIRLS mainly uses TREC and group tracking algorithms to forecast the distribution of precipitation. A key

* Corresponding author at: State Key Laboratory of Severe Weather, Chinese Academy of Meteorological Science, 46 Zhongguancun South Street, Haidian District, Beijing 100081, China.
E-mail address: wgl3111@camscma.cn (G. Wang).

http://dx.doi.org/10.1016/j.atmosres.2016.06.004

development of SWIRLS is that it uses a time-adjusted reflectivity–rainfall relationship from radar and rain gauge data for monitoring and predicting local rainfall distribution trends with a lead time of about two hours.

The "spin-up" problem has significantly affected the application of NWP models for nowcasting of precipitation (Daley, 1991). Recently, the spin-up effect has been significantly reduced with the development of high-performance computer systems and data assimilation techniques. Recent investigations have shown that a NWP model with suitable data assimilation can significantly improve short-term precipitation forecasts by assimilating radar reflectivity or Doppler velocity (Macpherson, 2001; Weygandt et al., 2002; Caya et al., 2005; Tong and Xue, 2005; Sokol, 2007). The high-resolution rapid refresh (Zahraei et al., 2012) developed by the National Oceanic and Atmospheric Administration and the ARPS used at the Center for Analysis and Prediction of Storms (CAPS) have been operationally applied for nowcasting precipitation. However, NWP forecasts may not be optimal for very short lead times because they mainly depend on the initial field and boundary conditions (Benjamin et al., 2004).

A nowcasting system referred to as BJ-ANC and a storm-scale NWP model of ARPS have been operationally run for precipitation forecasts in Jiangsu Observatory. BJ-ANC originated from the ANC, which was developed by the National Center of Atmospheric Research (NCAR), and was first implemented by the Beijing Meteorological Bureau, Chinese Meteorological Administration (CMA) for meteorological services during the 29th Olympic Games held in Beijing, China in 2008. The ARPS model was developed by CAPS at the University of Oklahoma in the United States. The Jiangsu Observatory introduced the ARPS model from CAPS to provide better weather services during the second Youth Olympics Games held in Nanjing, China in 2014. The evaluation and comparison of the two schemes are performed for hourly precipitation forecasts at lead times from 1 to 6 h. Six heavy precipitation events that occurred during the summer of 2014 and 2015 in Jiangsu were selected in this study. Such events usually occur during summer in Jiangsu, and they are frequently accompanied by floods that cause significant economic losses and even casualties. Thus, forecasting these events is very important for warning and emergency response.

The paper is organized as follows. A short overview of the datasets and the six heavy precipitation events used in this study are given in Section 2. The ARPS model and BJ-ANC systems are introduced in Sections 3 and 4, respectively. The methods implemented for forecast verification are described in Section 5, and the results of the evaluation and comparisons of the two forecast schemes based on the six heavy rain events are presented in Section 6. The conclusions and discussions are given in Section 7.

2. Data and case study

Fig. 1 presents the study domain and indicates where the observation data from radars and rawinsondes were derived in this study. The positions of automatic weather stations (AWSs) are not given for their high density. The radar data was acquired from CMA radar network with 6-min temporal resolution. The single radar reflectivity data underwent quality control to remove nonprecipitation targets including ground clutter, electronic interference, and anomalous propagations. Considering single radar is limited for covering widespread rain, the composite radar reflectivity mosaics from the six radars in Jiangsu at an elevation of 3 km above sea level with a spatial resolution of 0.01° were used to track and nowcast reflectivity fields. Quantitative precipitation estimations (QPEs) radar-based are calculated using the local radar reflectivity–rainfall rate (Z–R) relationship of $R = 386R^{1.43}$. The AWS data have a resolution of ~10 km and consists of temperature, pressure, humidity, wind, and precipitation. The three rawinsonde stations in Jiangsu are located in Xuzhou, Sheyang, and Nanjing. Measurements are available daily at 0800 and 2000 Beijing time (BJT).

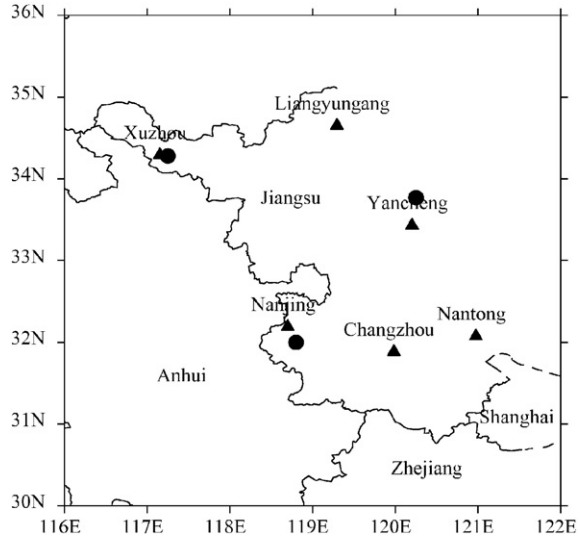

Fig. 1. The study domain and locations of Doppler radars (triangles) and rawinsonde stations (circles).

Climatologically, heavy precipitation events usually occur during summer and are affected by the Meiyu front in Jiangsu, potentially causing local flash floods. From an operational perspective, these forecast schemes are beneficial for extreme precipitation events. Therefore, six heavy rain events that occurred during summer were selected to verify and compare the forecast performances of BJ-ANC and ARPS. Representative QPEs radar-based with 6-hour intervals on one day for each event are shown in Fig. 2. The first event occurred on June 1, 2014. This event was quite extensive and relatively dominated by convective clouds and was companied with lightning and gust. The second event observed on June 24, 2014, and exhibited relatively light and scattered precipitation. The third event was clearly a large storm that occurred on August 13, 2014. This storm was dominated by convective activities, damaged more than 60 homes, and resulted in economic losses amounting to more than 20 million RMB. The fourth, fifth, and sixth events occurred during the summer of 2015 and were all intense, prolonged convective systems that destroyed homes and caused serious economic losses. Among the three heavy rain events, the disaster from the fifth event was the most serious, affecting about one million people, with one death, and economic losses of 2.1 billion RMB.

3. Advanced regional prediction system (ARPS)

The ARPS is a state-of-the-art storm-scale forecasting model developed by the CAPS at the University of Oklahoma, USA (Xue et al., 2000, 2001, 2003). The ARPS model is a compressible non-hydrostatic model and predicts 3D wind velocity vectors (u, v, and w); pressure (p); turbulent kinetic energy (TKE); potential temperature (θ); water vapor mixing ratio (q_v); and the mixing ratios of cloud water, rainwater, ice, snow, and hail (q_c, q_r, q_i, q_s, and q_h, respectively). A $243 \times 243 \times 53$ grid with a horizontal resolution of 3 km defines the whole physical domain of Jiangsu. In the vertical, a grid stretching scheme based on a cubic function is used in the vertical direction with a mean vertical resolution of 400 m and a high resolution of 20 m at the surface. The ARPS model used a 3-ice microphysical scheme (Lin et al., 1983). Subgrid-scale turbulence mixing was handled by the 1.5-order TKE-based turbulence parameterization following Deardorff (1980), whereas within the convective planetary boundary layer, a nonlocal vertical mixing length was calculated following Sun and Chang (1986).

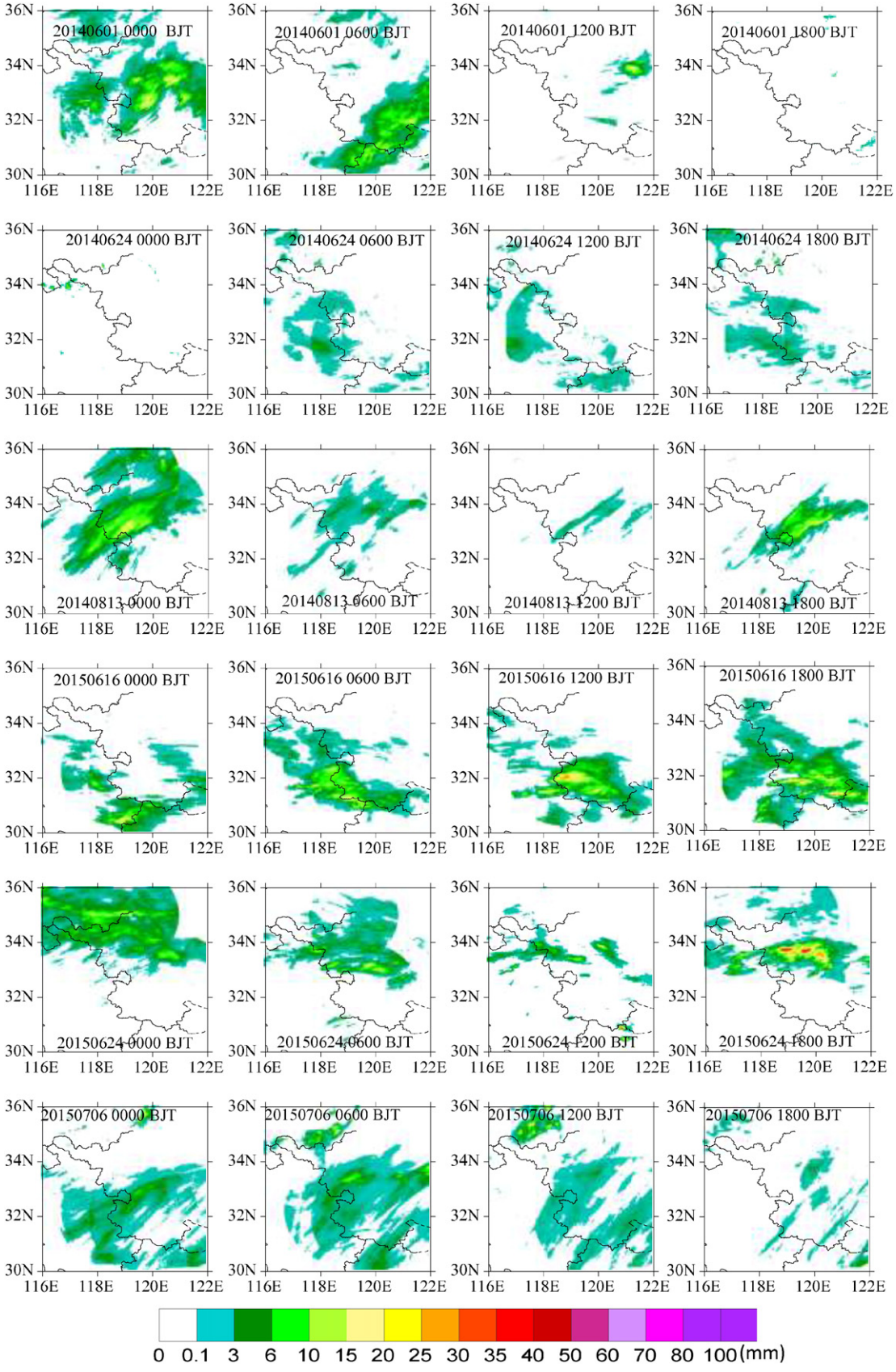

Fig. 2. Precipitation images (with the spatial resolution of 0.01° × 0.01°) of 1-h QPE of the six heavy rain events used in this study.

Other choices for the model dynamics include fourth-order momentum advection used in both the horizontal and vertical directions. A fourth-order monotonic flux-corrected transport scheme (Zalesak, 1979) was applied to potential temperature, water variables, and TKE. Details on these physics and computational options can be found in Xue et al. (2000, 2001, 2003).

The Jiangsu Observatory introduced the ARPS model from the CAPS to support the weather services and provide the short-range numerical weather forecast during the second Youth Olympics Games held in Nanjing, China in 2014. The radar observations including radar radial velocity and reflectivity factor are assimilated with a Palysis system (Gao et al., 2004; Brewster, 2003; Hu et al., 2006a, 2006b) within the ARPS to obtain the initial conditions. The ARPS was operationally run in Jiangsu Observatory and initialized every 3 h to provide forecasts up to 24 h with a high spatial resolution of 3 km × 3 km and temporal intervals of 1 h.

4. Beijing auto-nowcast system (BJ-ANC)

The BJ-ANC was modified from the ANC developed by NCAR, which produces up to 1-h nowcasts of convective storm location and intensity with high spatial and temporal resolution (Mueller et al., 2003). To support better meteorological services during the 29th Olympic Games held in Beijing, China in 2008, the ANC was introduced, then improvements and further modifications to many of its key algorithms and modules was made to adapt local weather feature. The localized

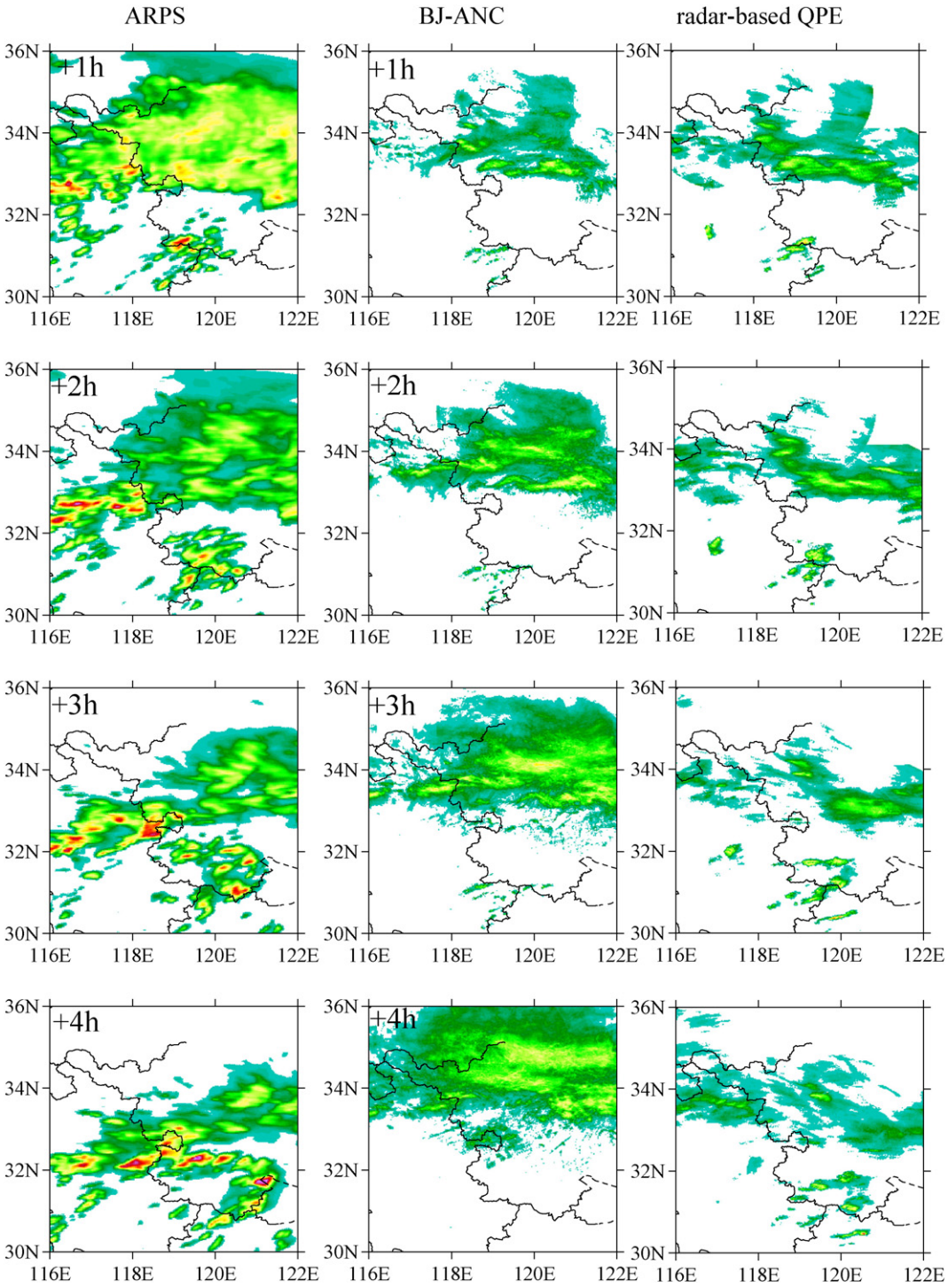

Fig. 3. Comparison of forecasted precipitation by the ARPS (left column) and BJ-ANC (middle column) initialized at 0600 BJT 24th June 2015 from 1 to 6 h lead times at the spatial scale of 0.01° × 0.01°, and the corresponding radar observations (right column).

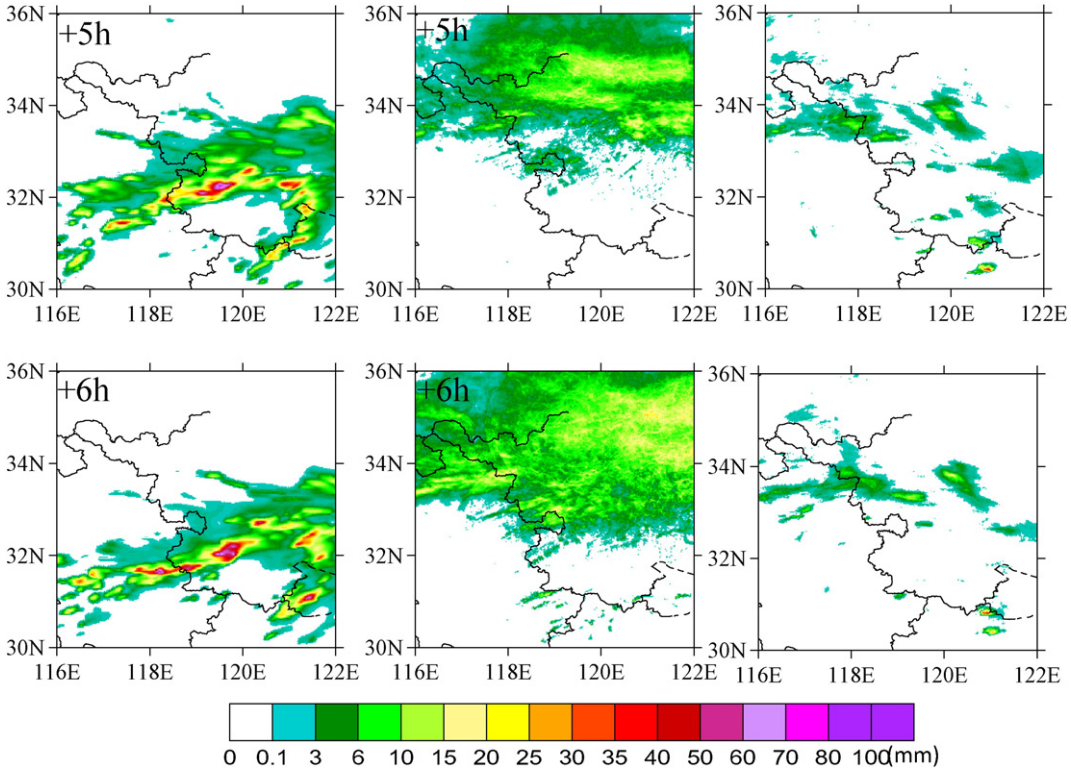

Fig. 3 (*continued*).

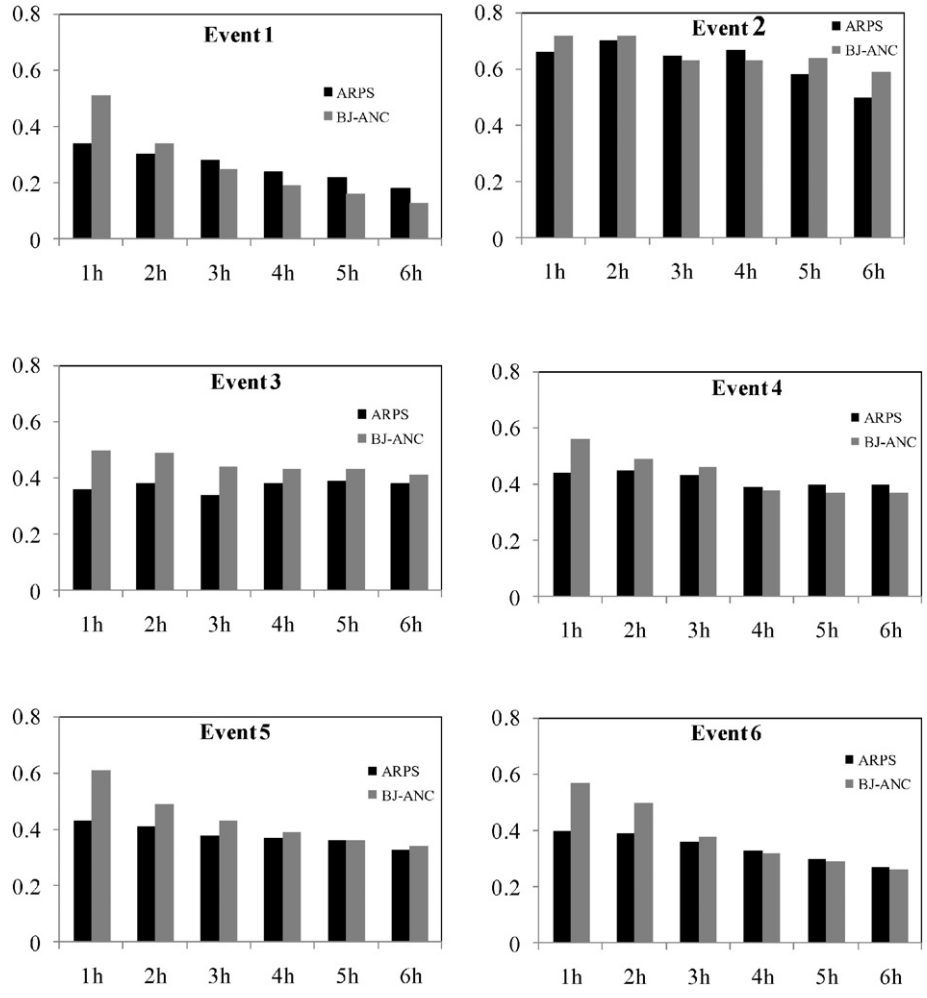

Fig. 4. CSI of the ARPS and BJ-ANC at lead times from 1 to 6 h for each event.

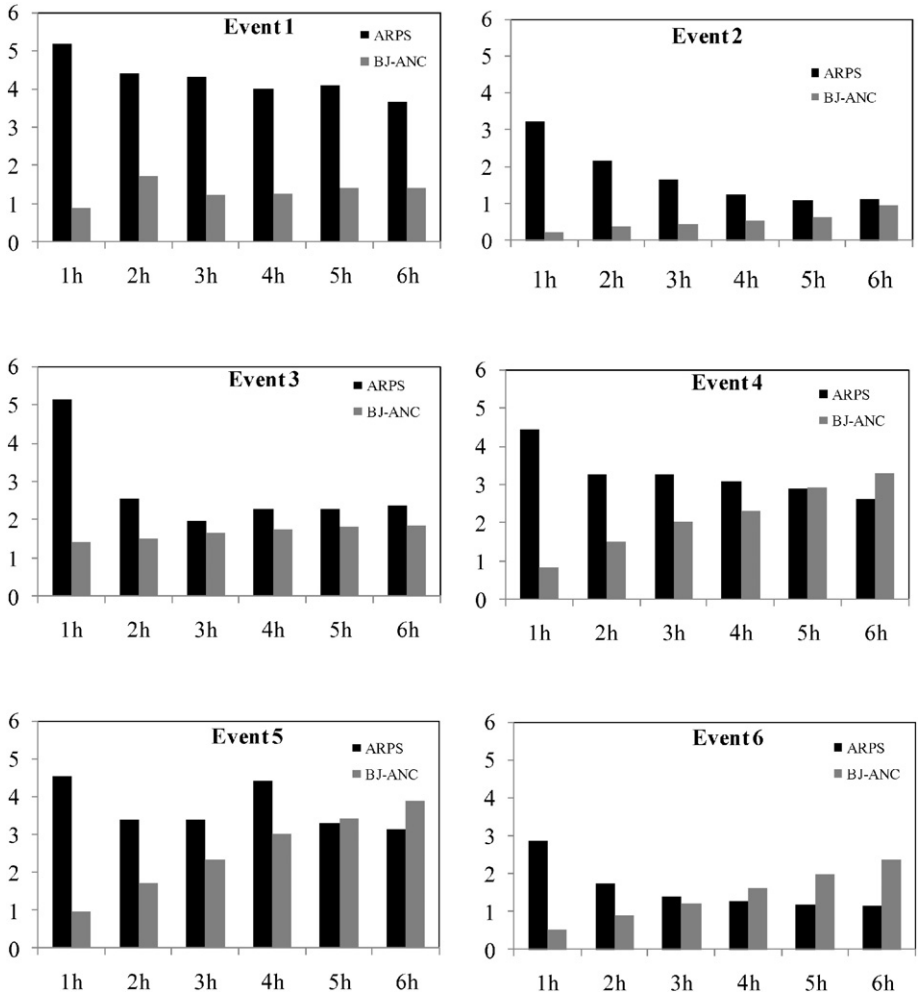

Fig. 5. RMSE of the ARPS and BJ-ANC at lead times from 1 to 6 h for each event.

nowcasting system was referred to as the BJ-ANC. Key improvements to the algorithms included quality control of radar data, analysis and diagnosis of local observations from radars, AWSs, rawinsondes, identification and tracking of storm cells, grid-based tracking and extrapolation of radar echo, assimilation of radar data, QPE, and QPF (Chen et al., 2010). The initiation and evolution of the storm is predicted

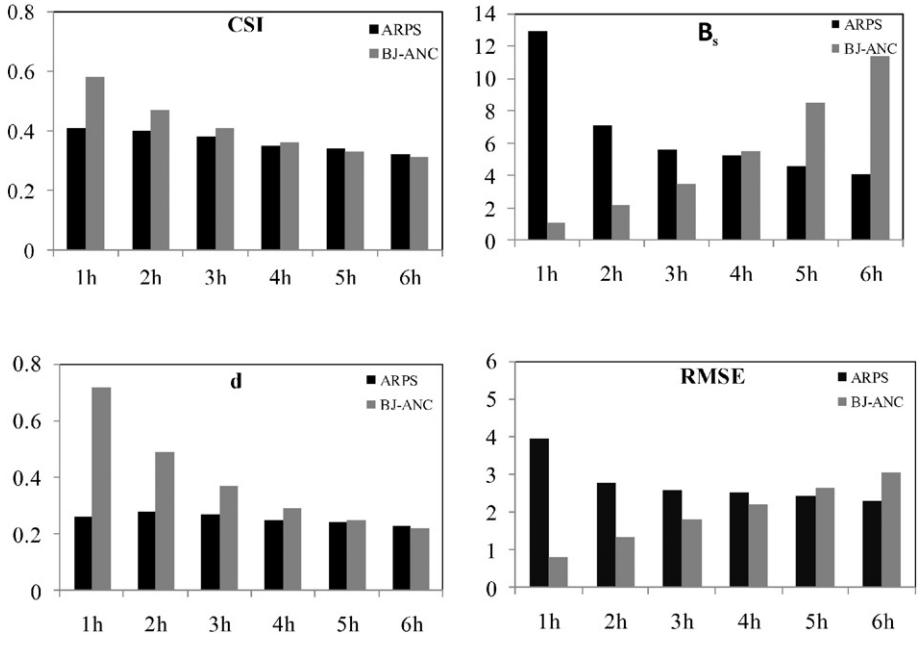

Fig. 6. Average forecast performance indices over the six considered heavy precipitation events at lead times from 1 to 6 h.

based on boundary layer information and cloud characteristics. These algorithms generate several predictor fields, which are combined by a fuzzy logic routine to nowcast 0–1 h storm location and intensity (Mueller et al., 2003; Chen et al., 2010).

The BJ-ANC system ran in real time during the summer of 2008. Its performance was improved after boundary layer convergence lines were entered by a human–computer interactive function. Evaluation of 1-h extrapolations of storms and QPFs in Beijing and its vicinity during the summer of 2008 was performed using the Beijing 2008 Forecast Demonstration Project real-time verification system. The results show that the BJ-ANC is highly capable of nowcasting storm initiation, growth, and dissipation supported by boundary layer information. In addition, the retrieval of thermodynamic fields can also reveal 3D wind structures, convergence, and temperature at low atmospheric layers and further help forecasters with predicting storm initiation and evolution (Chen et al., 2010).

Germann and Zawadzki (2002) have shown that the range of predictability increases with increasing scale. Due to most heavy precipitation events with prolonged period during summer in Jiangsu, the BJ-ANC was expanded to forecast precipitation with lead times up to 6 h by adjusting some parameters and has been run in the Jiangsu Observatory (Cheng et al., 2013). The BJ-ANC outputs hourly precipitation forecast up to 6 h every 6 min and horizontal resolution of 0.01° × 0.01°.

5. Forecast verification methods

The aims of the study are to evaluate the QPF performances of the ARPS and BJ-ANC and compare their forecasting accuracy. The outputs of ARPS and BJ-ANC differ in their positions (the ARPS uses the rotated geographic coordinates and the BJ-ANC uses the Cartesian coordinates) and resolutions. To verify and compare the forecasts, the ARPS outputs are transformed into Cartesian coordinates as the BJ-ANC using Lambert projection, and interpolated into the same resolution as the BJ-ANC by the NCAR Command Language (NCL). The second difference is temporal resolution. The ARPS model is initialized operationally every 3 h and forecasts up to 24-h lead times with 1-h intervals. The BJ-ANC forecasts hourly precipitation fields up to 6-h ahead every 6 min. To comparison, the ARPS forecasts up to 6-h lead times were chosen, and the BJ-ANC forecasts from the same base time as the ARPS were selected. The corresponding radar-based QPEs were used to verify and compare the forecasts by the BJ-ANC and ARPS.

Because of the variability of precipitation fields, there is no uniform verification method to evaluate all forecast features (Sokol et al., 2013). Gridpoint-based measures and object-based verification were applied in this study. The gridpoint-based measures compare forecasts and observations in the same grids, which is appropriate for evaluating synoptic-scale precipitation but is limited by the "double penalty problem" for precipitation fields with complex structures (Wernli et al., 2008). Four performance indices in the gridpoint-based measures were used in this study. The critical success index (CSI) measures the patterns match between forecasts and observations. Bias (B_s) measures the ratio between forecasted and observed rainfall. Considering that the correlation coefficient is insensitive to linear differences between the observations and predictions, an agreement index (d) was used to measure the agreement between forecasts and observations (Legates and McCabe, 1999). The root mean square error (RMSE) was calculated to evaluate the quantitative error. The formulas are defined as follows.

$$CSI = \frac{n_s}{n_s + n_f + n_a} \tag{1}$$

$$B_s = \frac{\sum_{i=1}^{N} F_i}{\sum_{i=1}^{N} O_i} \tag{2}$$

$$d = 1 - \frac{\sum_{i=1}^{N} (O_i - F_i)^2}{\sum_{i=1}^{N} \left(|O_i - \overline{O}| + |F_i - \overline{O}| \right)^2} \tag{3}$$

$$\mathrm{RMSE} = \sqrt{\frac{\sum_{i=1}^{N} (O_i - F_i)^2}{N}} \tag{4}$$

where O_i and F_i are the observed and predicted rainfall amounts at the ith grid point, and the bar indicates the mean value. N is the number of observations and forecasts, and n_s, n_f, and n_a denote the number of successes, failures, and false alarms, respectively. When the observed and predicted rainfall are equal, then a perfect forecast would yield CSI = 1, B_s = 1, d = 1, and RMSE = 0. The concepts of success, failure, and false alarms are the same as those used in the literature (Grecu and Krajewski, 2000; Zahraei et al., 2012).

To identify the sources of forecast errors, an object-based measurement method referred to as SAL, which considers three components of the structure (S), amplitude (A), and location (L) of the precipitation field, was developed by Wernli et al. (2008) to verify QPF. This measure supplements the evaluation of forecasts related to the gridpoint-based measurement method, but it provides little insight on the quantitative accuracy of forecasts (Sokol et al., 2013).

The components structure (S) and location (L) evaluates predicted precipitation fields based on precipitation objects, which are defined as coherent grids with precipitation values greater or equal to a threshold within the chosen domain. The structure component (S) compares the volume of the predicted and observed precipitation

Table 1
Mean Bs of the two forecasting schemes for six heavy rain events.

Event	Schemes	Lead times					
		1 h	2 h	3 h	4 h	5 h	6 h
1	ARPS	16.65	17.44	20.14	18.45	14.99	15.98
	BJ-ANC	0.91	1.51	2.33	3.55	4.02	6.09
2	ARPS	18.65	4.05	2.29	2.72	1.67	1.29
	BJ-ANC	5.05	4.25	4.06	4.86	3.37	2.51
3	ARPS	20.28	9.28	5.34	6.41	6.01	5.70
	BJ-ANC	2.66	2.94	3.64	3.98	4.41	5.15
4	ARPS	12.72	7.05	6.90	5.70	5.40	4.57
	BJ-ANC	0.96	1.98	3.27	4.23	7.96	12.35
5	ARPS	10.77	6.12	4.69	4.76	4.42	3.87
	BJ-ANC	1.03	2.01	3.1	5.00	6.87	8.79
6	ARPS	14.00	6.52	4.18	3.50	2.93	2.45
	BJ-ANC	1.04	2.33	4.02	7.00	11.07	14.57

Table 2
Mean index of agreement of the two forecasting schemes for six heavy rain events.

Event	Schemes	Lead times					
		1 h	2 h	3 h	4 h	5 h	6 h
1	ARPS	0.2	0.14	0.12	0.07	0.06	0.06
	BJ-ANC	0.65	0.34	0.23	0.17	0.12	0.10
2	ARPS	0.10	0.14	0.16	0.21	0.28	0.26
	BJ-ANC	0.63	0.65	0.69	0.42	0.42	0.29
3	ARPS	0.21	0.29	0.31	0.24	0.24	0.24
	BJ-ANC	0.53	0.46	0.38	0.34	0.30	0.30
4	ARPS	0.27	0.27	0.25	0.24	0.28	0.27
	BJ-ANC	0.75	0.50	0.38	0.30	0.30	0.26
5	ARPS	0.30	0.30	0.28	0.26	0.23	0.22
	BJ-ANC	0.74	0.50	0.36	0.30	0.24	0.22
6	ARPS	0.24	0.28	0.28	0.26	0.25	0.24
	BJ-ANC	0.72	0.48	0.38	0.28	0.24	0.21

fields. Positive (negative) value of S indicates widespread (sharp) predicted precipitation fields. The amplitude component (A) corresponds to the mean precipitation difference between the forecasts and observations over the chosen domain. The value of A shows whether the predicted precipitation is overestimated or underestimated, and the calculation of A is independent of the precipitation objects and the given threshold. The location component (L) consists of two segments: the first segment measures the distance between the centers of mass of the forecasted and observed precipitation fields within the chosen domain, and the second segment measures the mean distance between the centers of the total precipitation field and individual precipitation objects. Definitions and details of the three components are provided in Wernli et al. (2008). A perfect forecast would result in $S = 0$, $A = 0$ and $L = 0$.

An area-growing method was used to identify coherent grids with precipitation values greater or equal to a threshold as an individual precipitation object. The "area-growing method" was also used to identify storms by Lakshmanan (2001). Considering that the SAL results were not sensitive to the threshold, we used the same approach that as reported by Wernli et al. (2008) to choose a threshold.

$$R^* = fR^{\max} \tag{5}$$

where R^* denotes the threshold and R^{max} is the maximum precipitation value within the chosen domain. f is a coefficient and was set to 1/15, which is the same coefficient used by Wernli.

6. Results and discussion

Six heavy rainfall events presented in Fig. 2 were selected for verification and comparison of the forecast performances of the BJ-ANC system and ARPS model.

Fig. 3 shows an example of the hourly precipitation distribution forecasted by the ARPS model and BJ-ANC system at lead times from 1 to 6 h with 1-h intervals at a base time of 0600 BJT on June 24, 2015, and corresponding radar-based QPEs. In general, the forecasted position

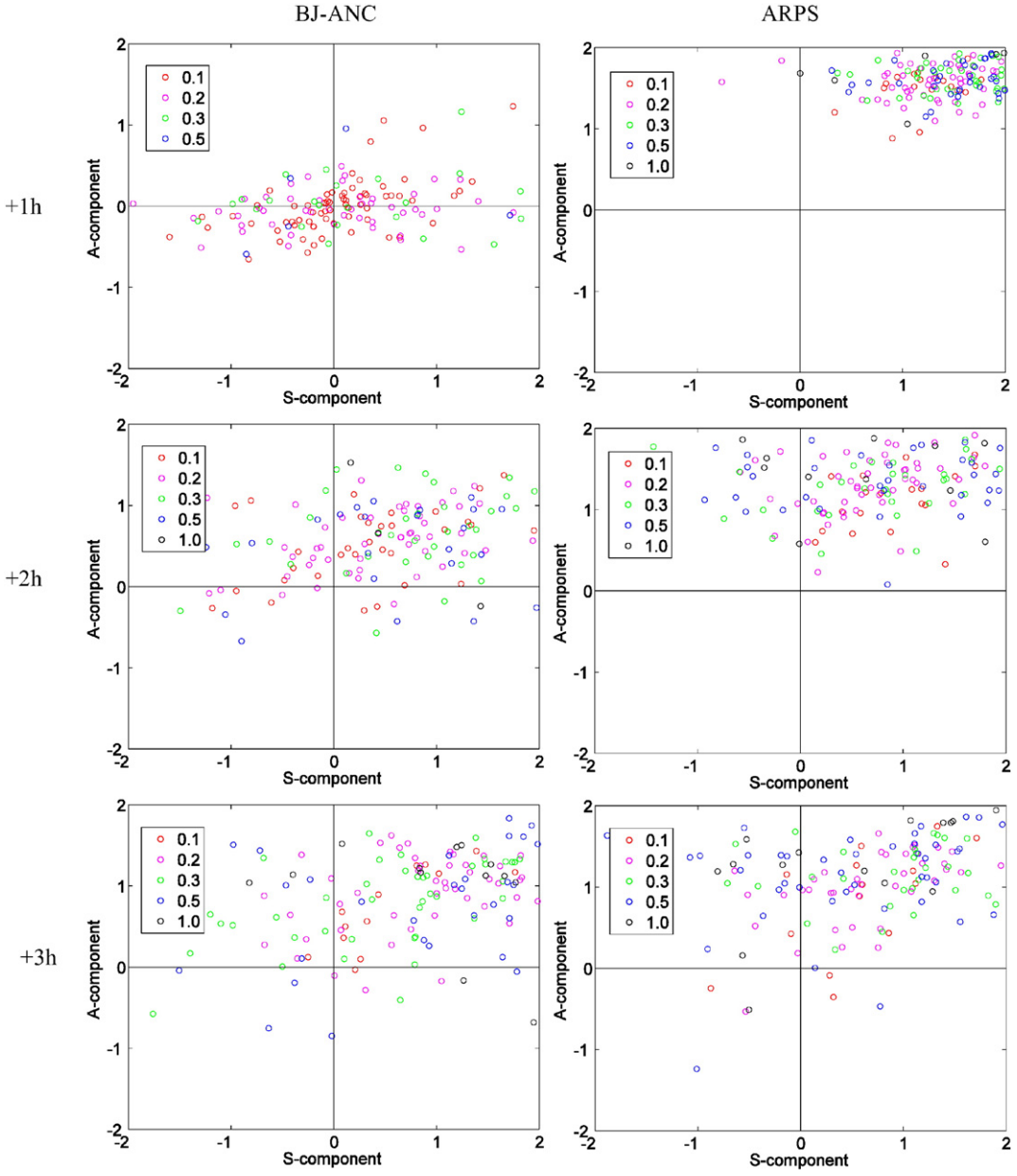

Fig. 7. SAL diagrams for the hourly precipitation forecasts of the ARPS (left column) and BJ-ANC (right column) at lead times from 1 to 6 h. Every circle indicates three components of SAL for a forecast. The L component is indicated by the color of the circles.

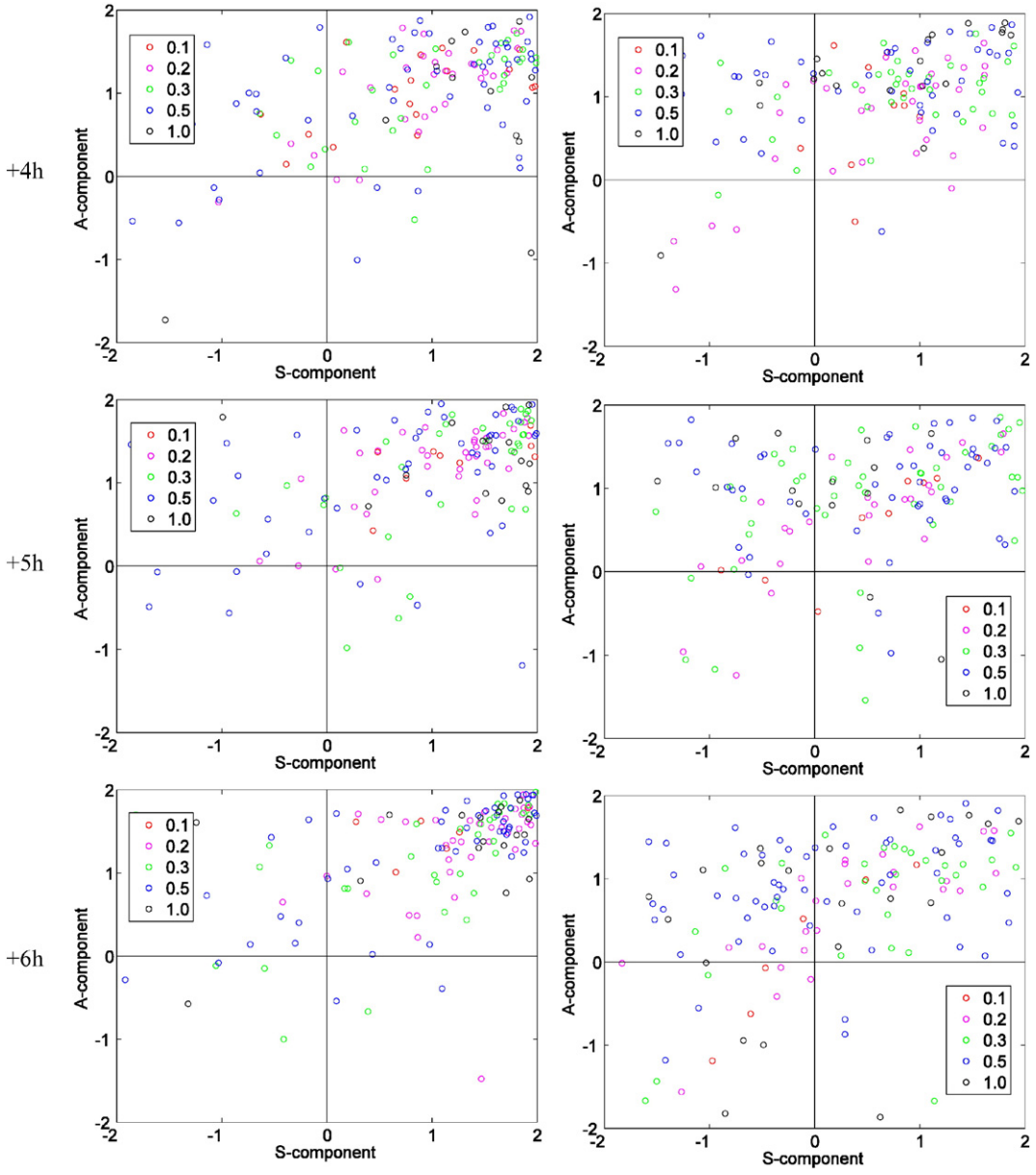

Fig. 7 (*continued*).

of precipitation by the two schemes matches well with that of the observed radar-based QPEs. As indicated, the ARPS forecasts overestimate precipitation amounts and precipitation area compared with the observations at 1-h lead time. However, the forecasting skill improved gradually with increasing lead time. The BJ-ANC system outperforms the ARPS model and comparisons with the observations are satisfactory with short lead times, but apparently the BJ-ANC system does not accurately predict the evolution of precipitation and its forecasting skill decreases rapidly with increasing lead time. Fig. 3 shows that according to radar-based QPEs, precipitation gradually weakened, whereas the precipitation predicted by the BJ-ANC gradually strengthened, leading to increased overestimations and widespread precipitation with lead time.

Figs. 4–6 and Tables 1–2 show quantitative results of the ARPS and BJ-ANC for lead times of 1–6 h and a comparison of their outputs by gridpoint-based measures for each event. In general, the BJ-ANC performs better than the ARPS at short lead times, which is confirmed by all the chosen performance indices related to grindpoint-based measures. However, the performance of BJ-ANC decreases rapidly with lead time.

To obtain meaningful verification and comparison of the results, average performance indices over the six selected heavy rain events are given in Fig. 6. The indices reveal that the BJ-ANC has better CSI (0.61) than the ARPS (0.43) for lead times of 1 h. However, the CSI of the BJ-ANC reduces rapidly, whereas that of the.

ARPS changes little over the forecast period. Moreover, the ARPS has a better CSI than the BJ-ANC for over 5-h lead times. In regard to Bs and RMSE, the BJ-ANC outperforms ARPS for forecasts with 4–5-h

Table 3
Mean values of S-component, A-component and L-component of the two forecasting schemes over six heavy rain events.

Lead Times	S(ARPS)	S(BJ-ANC)	A(ARPS)	A(BJ-ANC)	L(ARPS)	L(BJ-ANC)
1 h	1.35	0.06	1.59	0.00	0.23	0.13
2 h	0.68	0.48	1.29	0.56	0.25	0.19
3 h	0.56	0.70	1.07	0.84	0.29	0.25
4 h	0.61	0.86	1.01	1.01	0.31	0.28
5 h	0.45	0.99	0.87	1.14	0.31	0.29
6 h	0.22	1.04	0.73	1.23	0.34	0.30

lead times, after which the ARPS performs better than the BJ-ANC. The BJ-ANC outperforms ARPS in terms of the agreement index except for the lead time of 6 h.

Evaluation of the BJ-ANC and ARPS by SAL based on the six considered heavy rain events is shown in Fig. 7. Most BJ-ANC forecasts are indicated by the red and purple dots around the center of the diagram at a lead time of 1 h, which represents a high-quality forecast. This is also confirmed when both mean A and S are close to 0 and L has a low value (Table 3). However, as the lead time increases, most forecasts focus on the first (top right) quadrant of the diagram, which implies that the BJ-ANC forecasts overestimate both the structure and amplitude of precipitation. Table 3 shows that the mean values of the components S, A, and L, which are all positive and increase with lead time. Further analysis shows that in most cases a decrease in precipitation was observed, but the BJ-ANC predicted an enhancement in precipitation. Conversely, most ARPS forecasts are characterized by positive A values, implying an overestimation in the ARPS-derived precipitation. Especially for a lead time of 1 h, the greater density of dots in the top right-hand corner of the diagram indicates that the ARPS produced too large precipitation amounts and significantly overestimated precipitation objects. As the lead time increases, some forecasts can be seen in the second quadrant of the diagram, which means that the ARPS predicted overestimated precipitation with too small and/or too sharp precipitation objects. As shown in Table 3, both the mean values of S and A decrease with lead time, whereas the mean value of L increases slightly with lead time.

7. Summary and conclusions

Two precipitation forecasting schemes, one applying the NWP model with atmospheric dynamic constraints, and the other one combining an extrapolation of observed radar images and with application of initiation and evolution of storms based on boundary layer convergence and thermodynamic fields, were validated and compared based on six heavy rain events that occurred during the summer of 2004 and 2005 in Jiangsu. The forecast performances were evaluated and compared as a function of lead times in the range of 1 to 6 h using gridpoint-based and object-based measures.

Even with atmospheric dynamic constraints and data assimilation techniques, the ARPS may not produce optimal forecasts for very short lead times. The storm-scale NWP model still has some limitations for very short-term forecast of precipitation.In general, the ARPS model yields overestimated and widespread precipitation at a lead time of 1 h, which was confirmed by the significantly large bias and that most forecasts were concentrated in the top right-hand corner of the SAL diagram. The forecasting skill gradually improves with lead time, but the ARPS overestimates precipitation at all of the considered lead times. The systematic error of overestimated precipitation may be corrected by statistical methods. Conversely, the BJ-ANC produces a high quality forecast at a lead time of 1 h, but its performance degrades rapidly with lead time. Applying a boundary layer convergence line and thermodynamic fields, in most cases, the BJ-ANC inaccurately predicts storm evolution of storms and therefore yields significant precipitation both in amplitude and extension over time following the initial forecast. A decrease in the accuracy of the BJ-ANC forecasts with increasing lead time is evident by its inaccurate prediction of storm evolution.

The ARPS and BJ-ANC have individual advantages and limitations. The BJ-ANC performs better than the ARPS at very short lead times, whereas the ARPS outperforms the BJ-ANC after several hours of the initial forecast. The cross-over point occurs at about an elapsed time of 4–5 h following the initial forecast. It seems that correcting the ARPS forecasts and subsequently merging the two schemes may be a viable path for improving QPFs within 0–6 h, which have been developed in recent years (Wilson and Xu, 2006; Bowler et al., 2006; Wong et al., 2009) and what we urge the community to work on.

Acknowledgments

This study was supported by Beijige Fund of Jiangsu Institute of Meteorological Science (Grant No. BJG201303). The authors would also acknowledge Jiangsu Observatory for providing the datasets used in the study.

References

Benjamin, S.G., Devenyi, D., Weygandt, S.S., Brundage, K.J., Brown, J.M., Grell, G.A., Kim, D., Schwartz, B.E., Smirnova, T.G., Smith, T.L., Manikin, G.S., 2004. An hourly assimilation-forecast cycle: the RUC. Mon. Weather Rev. 132, 495–518.
Bowler, N., Pierce, C., Seed, A., 2006. STEPS: a probabilistic precipitation forecasting scheme which merges an extrapolation nowcast with downscaled NWP. Q. J. R. Meteorol. Soc. 132, 2127–2155.
Brewster, K.A., 2003. Phase-correcting data assimilation and application to storm-scale numerical weather prediction. Part I: method description and simulation testing. Mon. Weather Rev. 131, 480–492.
Caya, A., Sun, J., Snyder, C., 2005. A comparison between 4D Var and the ensemble Kalman filter technique for radar data assimilation. Mon. Weather Rev. 133, 3081–3093.
Chen, M.X., Gao, F., Kong, R., Wang, Y.C., Wang, J.J., Tan, X.G., Xiao, X., Zhang, W.L., Wang, L., Ding, Q.L., 2010. Introduction of auto-nowcasting system for convective and its performance in Beijing Olympics meteorological service. J. Appl. Meteorol. Sci. 21 (4), 395–404 (in Chinese).
Cheng, C.L., Chen, M.X., Wang, J.J., Gao, F., Yang, H.X., 2013. Short-term quantitative precipitation forecast experiments based on blending of nowcasting with numerical weather prediction. Acta Meteorol. Sin. 71 (3), 397–415 (in Chinese).
Daley, R., 1991. Atmospheric Data Analysis. Cambridge University Press (457 PP.).
Deardorff, J.W., 1980. Stratocumulus-capped mixed layers derived from a three-dimensional model. Bound.-Layer Meteorol. 18 (4), 495–527.
Dixon, M., Wiener, G., 1993. TITAN: thunderstorm identification, tracking, analysis and nowcasting–a radar-based methodology. J. Atmos. Ocean. Technol. 10, 785–797.
Gao, J., Xue, M., Brewster, K., Droegemeier, K.K., 2004. A three-dimensional variational data analysis method with recursive filter for Doppler radars. J. Atmos. Ocean. Technol. 21, 457–469.
Germann, U., Zawadzki, I., 2002. Scale-dependence of the predictability of precipitation from continental radar images. Part I: description of the methodology. Mon. Weather Rev. 130 (12), 2859–2873.
Germann, U., Zawadzki, I., 2004. Scale-dependence of the predictability of precipitation from continental radar images. Part II: probability forecasts. J. Appl. Meteorol. 43 (1), 74–89.
Grecu, M., Krajewski, W.F., 2000. A large-sample investigation of statistical procedures for radar-based short-term quantitative precipitation forecasting. J. Hydrol. 239, 69–84.
Hu, M., Xue, M., Brewster, K., 2006a. 3DVAR and cloud analysis with WSR-88D level-II data for the prediction of fort worth tornadic thunderstorms. Part I: cloud analysis and its impact. Mon. Weather Rev. 134, 675–698.
Hu, M., Xue, M., Gao, J., Brewster, K., 2006b. 3DVAR and cloud analysis with WSR-88D level-II data for the prediction of fort worth tornadic thunderstorms. Part II: impact of radial velocity analysis via 3DVAR. Mon. Weather Rev. 134, 699–721.
Johnson, J.T., MacKeen, P.L., Witt, A., Mitchell, E.D., Stumpf, G.J., Eilts, M.D., Thomas, K.W., 1998. The storm cell identification and tracking algorithm: an enhanced WSR-88D algorithm. Weather Forecast. 13, 263–276.
Lakshmanan, V., 2001. A Heirarchical, Multiscale Texture Segmentation Algorithm for Real-World Scenes (PhD thesis) University of Oklahoma, Norman, OK.
Legates, D.R., McCabe, G.J., 1999. Evaluating the use of goodnessof-fit measures in hydrologic and hydroclimatic model validation. Water Resour. Res. 35 (1), 233–241.
Li, P.W., Lai, E.S., 2004. Short-range quantitative precipitation forecasting in Hong Kong. J. Hydrol. 288, 189–209.
Lin, Y.L., Farley, R.D., Orville, H.D., 1983. Bulk parameterization of the snow field in a cloud model. J. Clim. Appl. Meteorol. 22, 1065–1092.
Macpherson, B., 2001. Operational experience with assimilation of rainfall data in the Met Office mesoscale model. Meteorog. Atmos. Phys. 76, 3–8.
Mueller, C., Saxen, T., Roberts, R., Wilson, J., Betancourt, T., Dettling, S., Oien, N., Yee, J., 2003. NCAR auto-nowcast system. Weather Forecast. 18, 545–561.
Pierce, C.E., Collier, C.G., Hardaker, P.J., Haggett, C.M., 2000. GANDOLF: a system for generating automated nowcasts of convective precipitation. Meteorol. Appl. 8, 341–360.
Rinehart, R., Garvey, E., 1978. Three-dimensional storm motion detection by conventional weather radar. Nature 273, 287–289.
Sokol, Z., 2007. Utilization of radar reflectivity for a very short range precipitation forecast. Czech Meteorol. Bull. 60, 136–146.
Sokol, Z., Kitzmiller, D., Pesice, D., Mejsnar, J., 2013. Comparison of precipitation nowcasting by extrapolation and statistical-advection methods. Atmos. Res. 123, 17–30.
Sun, W.Y., Chang, C.Z., 1986. Diffusion model for a convective layer. Part I: numerical simulation of convective boundary layer. J. Clim. Appl. Meteorol. 25, 1445–1453.
Tong, M., Xue, M., 2005. Ensemble Kalman filter assimilation of Doppler radar data with a compressible nonhydrostatic model: OSS experiments. Mon. Weather Rev. 133, 1789–1807.
Vila, D.A., Machado, L.A., Laurent, H., Velasco, I., 2008. Forecast and tracking the evolution of cloud clusters (ForTraCC) using satellite infrared imagery: methodology and validation. Weather Forecast. 23, 233–245.
Wernli, H., Paulat, M., Hagen, M., Frei, C., 2008. SAL — a novel quality measure for the verification of quantitative precipitation forecasts. Mon. Weather Rev. 136, 4470–4487.

Weygandt, S.S., Shapiro, A., Droegemeier, K.K., 2002. Retrieval of model initial fields from single-Doppler observations of a supercell thunderstorm. Part I: single-Doppler velocity retrieval. Mon. Weather Rev. 130, 433–453.

Wilson, J., Xu, M., 2006. Experiments in Blending Radar Echo Extrapolation and NWP for Nowcasting Convective Storms. Proceedings, Fourth European Conference on Radar in Meteorology and Hydrology, Barcelona, Spain, pp. 519–522.

Wong, W.K., Yeung, L., Wang, Y.C., Chen, M.X., 2009. Towards the blending of NWP with nowcast: Operation Experience in B08FDP. In World Weather Research Program Symposium on Nowcasting, Whistler, BC, Canada, 30 Aug–4 Sep 2009.

Xue, M., Droegemeier, K.K., Wong, V., 2000. The advanced regional prediction system (ARPS) — a multiscale nonhydrostatic atmospheric simulation and prediction tool. Part I: model dynamics and verification. Meteorog. Atmos. Phys. 75, 161–193.

Xue, M., Droegemeier, K.K., Wong, V., Shapiro, A., Brewster, K., Carr, F., Weber, D., Liu, Y., Wang, D.H., 2001. The advanced regional prediction system (ARPS) — a multiscale nonhydrostatic atmospheric simulation and prediction tool. Part II: model physics and applications. Meteorog. Atmos. Phys. 76, 143–165.

Xue, M., Wang, D.H., Gao, J.D., Brewster, K., Droegemeier, K.K., 2003. The advanced regional prediction system (ARPS), storm-scale numerical weather prediction and data assimilation. Meteorog. Atmos. Phys. 82, 139–170.

Zahraei, A., Hsu, K., Sorooshian, S., Gourley, J.J., Hong, Y., Lakshmanan, V., Bellerby, T., 2012. Quantitative precipitation nowcasting, a Lagrangian pixel-based approach. J. Atmos. Res. 118, 418–434.

Zalesak, S.T., 1979. Fully multidimensional flux-corrected transport algorithms for fluids. J. Comput. Phys. 31, 335–362.